Multi-GeV Electron Generation Using Texas Petawatt Laser

X. Wang, D. Du, S. A. Yi, S. Kalmykov, E. D'avignon, N. Fazel, R. Zagdzaj, S. Reed, P. Dong, W. Henderson, G. Dyer, A. Bernstein, E. Gaul, M. Martinez, G. Shvets, T. Ditmire, and M. Downer

Citation: AIP Conference Proceedings **1299**, 209 (2010); doi: 10.1063/1.3520315
View online: http://dx.doi.org/10.1063/1.3520315
View Table of Contents: http://scitation.aip.org/content/aip/proceeding/aipcp/1299?ver=pdfcov
Published by the AIP Publishing

Multi-GeV Electron Generation Using Texas Petawatt Laser

X. Wang, D. Du, S.A. Yi, S. Kalmykov, E. D'avignon, N. Fazel, R. Zagdzaj, S. Reed, P. Dong, W. Henderson, G. Dyer, A. Bernstein, E. Gaul, M. Martinez, G. Shvets, T. Ditmire and M. Downer

Department of Physics, University of Texas at Austin
Austin, TX 78712, USA

Abstract We present simulation results and experimental setup for multi-GeV electron generation by a laser plasma wake field accelerator (LWFA) driven by the Texas Petawatt (TPW) laser. Simulations show that, in plasma of density $n_e = 2 - 4 \times 10^{17}$ cm^{-3}, the TPW laser pulse (1.1 PW, 170 fs) can self-guide over 5 Rayleigh ranges, while electrons self-injected into the LWFA can accelerate up to 7 GeV. Optical diagnostic methods employed to observe the laser beam self-guiding, electron trapping and plasma bubble formation and evolution are discussed. Electron beam diagnostics, including optical transition radiation (OTR) and electron gamma ray shower (EGS) generation, are discussed as well.

Keywords: Multi-GeV, Laser plasma accelerator, Texas petawatt laser system
PACS: 52.38.Kd, **41.75.Jv, 52.70.Kz**

INTRODUCTION

With the development of chirped pulse amplification (CPA), multi-TW laser peak power and focused intensity over 10^{19} Wcm^{-2} have been reached. In this relativistic regime, laser pulses can generate a nonlinear "bubble" structure in underdense plasma, from which electrons are evacuated and an approximately spherical region full of ions is formed [1, 2]. This plasma bubble, with electric field gradient on the order of GV/cm, is a high-quality table-top laser-plasma accelerator (LPA) that has generated quasi-monoenergetic electron bunches up to 1GeV [3,4,5], with many potential applications in science and technology. However, unless external guiding mechanism is applied [6], the acceleration length of a TW-laser-driven LPA, determined by the laser focusing geometry, dephasing length and pump depletion length, is usually around several millimeters, which limits the energy gain to < 1GeV. Furthermore, tightly focusing the laser pulse (< 5μm) into plasma of density 10^{19}cm^{-2} can cause strong self-phase modulation (SPM) and filamentation [7], which destroys the stability of bubble propagation and further limits energy gain.

Recently recipes [8, 9] for high-energy electron generation with LPA have shown that electrons can be accelerated to multi-GeV by using ~PW laser in more tenuous plasma (10^{17}cm^{-3}). Under these conditions, the dephasing length and depletion length are increased to tens of centimeters, and nonlinearities such as SPM and filamentation are weaker . PW laser power is required to satisfy $P \geq P_{cr}$, where $P_{cr} = 17\omega_0^2/\omega_p^2$GW is the critical power for relativistic self-focusing, so that the drive pulse self-guides.

The Texas Petawatt (PW) laser pulse (1.1PW, 170fs [10]), the shortest among all PW lasers in operation, with f#/40 focus satisfies the conditions $P \geq P_{cr}$ and $1 < \omega_p\tau_l < 2\pi$ for relativistic self-focusing in plasma of density n_e ~10^{17}cm^{-3} without SPM instabilities. It reaches high intensity (~10^{19}Wcm^{-2}) at large focal spot (r_0 = 80μm) to reduce radial plasma wave effect and increase laser Rayleigh range up to centimeters. Therefore, laser wakefields generated by the TPW laser are well suited for multi-GeV electron acceleration.

In the first section of this paper, we summarize the main results of particle-in-cell (PIC) simulations of LPA driven by the TPW laser, using the code WAKE. Further details of these simulations are presented in a paper by S. Kalmykov in this volume. In the second section of this paper, the anticipated experiments are described.

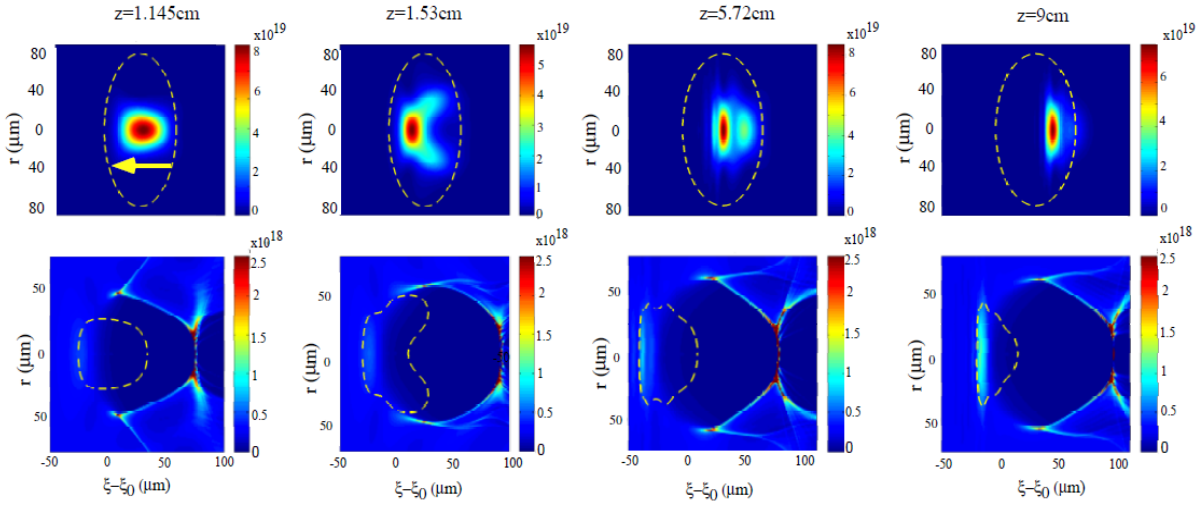

FIGURE 1. Evolution of TPW laser pulse and plasma structure in tenuous plasma ($10^{17}cm^{-3}$). Top row shows laser intensity profiles at four different positions (Z = 1.145cm, 1.53cm, 5.72cm, 9.0cm) in the gas cell. The dot line shows the original laser spot size and the arrow indicates laser propagation direction. Bottom row shows the plasma structure profile at the corresponding positions. The dotted line indicates the intensity profile of the laser pulse.

SUMMARY OF SIMULATION RESULTS

Fig.1 shows simulations results for the propagation of the TPW laser pulse (top row) and the bubble structure (bottom row) in plasma of density $n_e = 10^{17}cm^{-3}$. The laser pulse enters the He gas cell with radius $r_0 = 80\mu m$, then over-focuses down to radius $r_0 = 25\mu m$ within a Rayleigh range ($Z_R = 1.9cm$) due to relativistic self-focusing ($P/P_{cr} \sim 7$). It then expands to $r_0 = 40\mu m$ and propagates stably up to $5Z_R$, without significant variation of beam size, with relativistic self-focusing balancing vacuum diffraction. The laser pulse self-guides to 9cm with no filamentation or beam divergence. We confirmed that these favorable propagation characteristics are insensitive to imperfections --- *e.g.* hot spots, super-Gaussian profiles --- in the incident laser pulse profile.

Fig.1 also shows that a plasma bubble forms immediately after the laser pulse over-focuses (bottom row, left panel). This bubble structure subsequently contributes to stable self-guiding of the laser pulse. However, the initial over-focusing, subsequent expansion and re-focusing of the drive laser pulse causes corresponding small oscillations in the length of the bubble that are evident in the remaining bottom row panels of Fig. 1. These bubble length oscillations provide a key mechanism for injecting electrons from the ambient plasma into the bubble [11]. By contrast, a laser pulse that was better mode-matched to the plasma bubble, and experienced weaker oscillations, would be unable to capture electrons from such tenuous plasma. Thus drive laser over-focusing and bubble length oscillations are a fundamental component of the design of the TPW-LWFA experiment. Bubble expansion triggers electron injection, while subsequent bubble contraction terminates self-injection, enabling the TPW-LWFA to produce quasi-monoenergetic electrons.

Simulations of electron acceleration [9] (not shown in this paper) predict that 1nC, 7GeV, small divergence electron beam (6mrad.) with energy spread less than 10% can be generated within a 9cm self-guided TPW-LWFA in a tenuous plasma.

EXPERIMENTAL SETUP FOR TEXAS PETAWATT LASER WAKEFIELD ACCELERATOR

Fig. 2 shows the setup of the TPW LWFA experiment. An f#/40 concave spherical dielectric mirror (not shown) focuses the 1.1PW, 170fs, 1058nm laser pulses to r_0 = 80μm at the entrance to the He gas cell, located inside the experimental chamber. The intense (~10^{19} Wcm^{-2}, a_0 ~ 4) laser pulse creates and interacts with a low density, uniform He plasma (n_e ~ $10^{17}cm^{-3}$), generating an oscillating bubble that simulations predict will trap and accelerate electrons to several GeV, as described in the previous section.

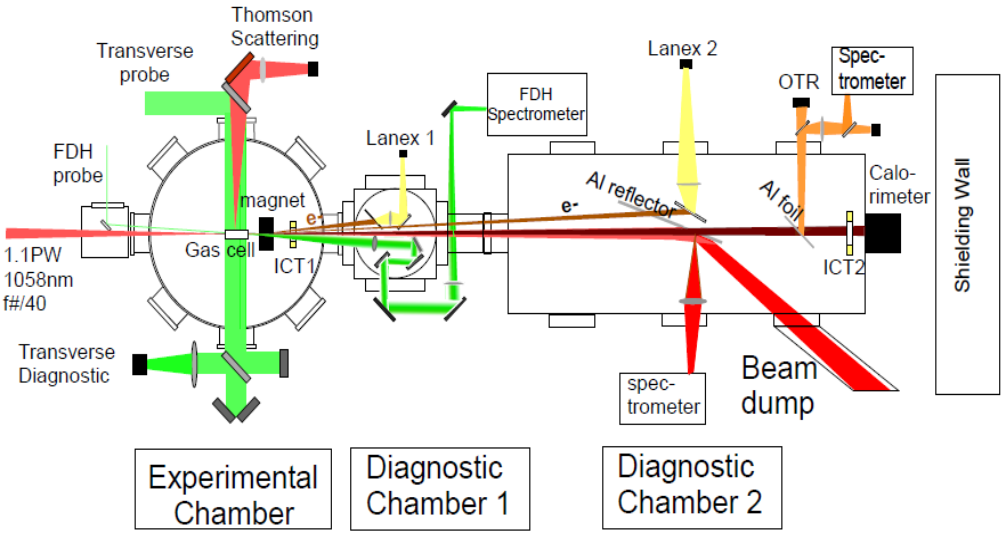

FIGURE 2. A schematic of the PW LWFA experiment setup.

To provide additional control over laser pulse over-focusing, bubble oscillation and electron self-injection, we have also designed an alternative gas cell with two chambers, as shown in Fig. 3, based on simulation results [9]. Chamber I is 5mm long and filled with mixture of He and N_2 gas, chamber II is 9cm long and filled with pure He gas. The five 2p shell electrons of nitrogen and 1s shell electron of a helium atom will be fully ionized by the PW laser at its incident intensity (~$10^{19}$$Wcm^{-2}$). The dense plasma slab in chamber I will thus act as an enhanced nonlinear plasma lens to over-focus the laser beam more strongly into the lower plasma density in chamber II. By selecting the proper percentage of nitrogen in the gas mixture, the focal spot can be optimized without filamenting. Chambers II and I are filled to equal pressures, thus minimizing interdiffusion and plasma density nonuniformity that can distort laser propagation in chamber II.

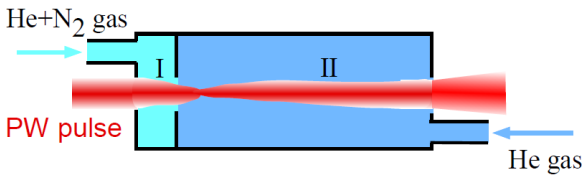

FIGURE 3. A gas cell for the TPW LWFA experiment.

A probe laser pulse, split off from laser beam in the front-end optical parametric amplifier (OPA) of the TPW system, will be used for optical diagnostics of laser-plasma interactions. The probe pulse, initially 1058nm, 30nm bandwidth, and chirped (2ns), passes through a delay line, is compressed to 50fs, then frequency doubled pulse (to 529nm) in a type I betas barium borate (BBO) crystal. The green probe is split into two beams, one for transverse diagnostics of the plasma, the other for frequency-domain holographic (FDH) visualization of the plasma bubble.

As shown in Fig.2, the transverse diagnostic beam is expanded to 9cm to cover the length of the self-guided laser path and formatted in a Milchelson interferometer to measure on-axis plasma density profile during the laser plasma interaction. The FDH beam, formatted into two pre-chirped 1ps laser pulses, reference and probe, with 3ps temporal separation, propagates at a 4.5 degree angle to the main PW beam, as shown schematically in Fig. 2 and 4(a). The plasma bubble sweeps across the probe beam and leaves a phase shift "streak" in it. The oscillations of the temporally evolving bubble can then be reconstructed from the interferogram generated by reference and probe pulse in frequency domain using Fourier transform methods described elsewhere [12]. Fig.4 (b) and (c) present simulations of the bubble's reconstructed phase streak based on the experimental conditions and configurations described above. Oscillations of the bubble's tail, which are critical to electron self-injection, are clearly visible. See the paper by Z. Li in this volume for further details of this frequency-domain streak camera method.

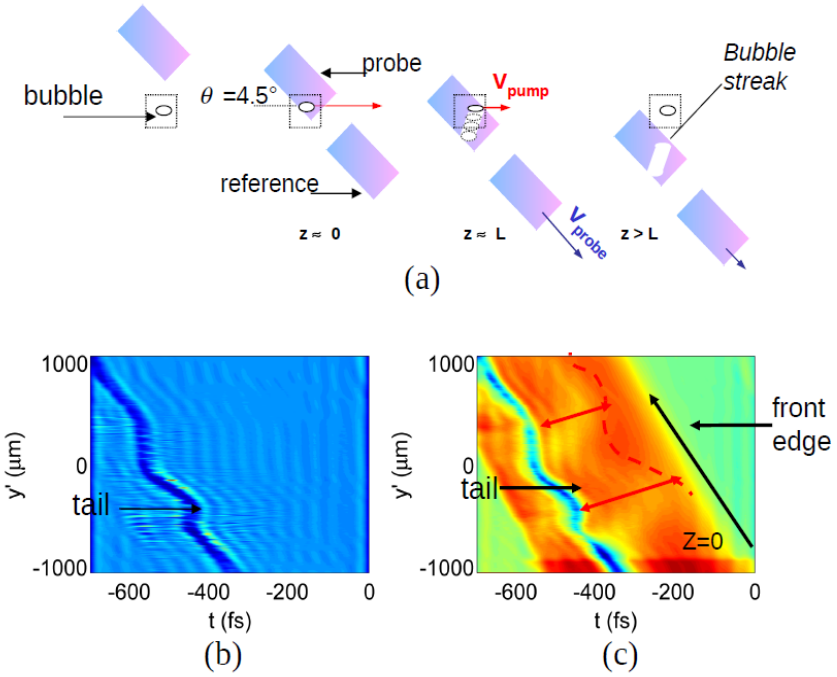

FIGURE 4. Schematic configurations for FDH (a) and simulation results of amplitude (b) and phase reconstruction (c). Black arrow in (a) denotes the propagation of main laser pulse. In (c), red dot line marks possible boundary of plasma bubble and black arrow denotes the direction of temporal evolution of bubble.

Incoherent side Thomson scattering (TS) of the main laser beam, as shown in Fig. 2, will be imaged to characterize laser self-guiding. The on-axis variation of TS light intensity, resulting from sequential diffraction and self-focusing, gives experimental evidence for laser self-guiding effect [13, 14]. Two 1 cm long sections, in the middle and at the end of the plasma, are selected and imaged on CCD cameras to study the laser beam evolution. Another image system is employed to image a 5mm section of the laser channel at the over-focused spot, which can be used to study the enhanced self-focusing effect caused by the nonlinear plasma lens described above.

As shown in Fig.2, the electron beam emerging from the gas cell propagates immediately through a 1Tesla dipole magnet to deflect sub-GeV electrons to Lanex1 and Lanex2 to measure up to 200MeV and up to 1GeV electrons, respectively. A 25μm Al deflector, which reflects the main laser pulse to a beam dump and transmits > 1 GeV electrons, separates the electron beam from main laser pulse. The electron beam penetrates another thin Al foil for optical transition radiation (OTR) and dumps into a calorimeter, described further below, which measures average electron energy in initial experiments. Two integrated current transformers (ICT) are located on the electron beam path to measure total charge of electrons and charge of high-energy electrons. Scattered main laser light from the Al deflector is collected and imaged to a spectrometer to measure spectral red shifts that evidence wakefield and guiding structure generation [15].

Optical transition radiation (OTR) occurs when the high-energy electrons transit the aluminum foil. In this experiment, visible and near infrared light (400nm-1100nm) emission from OTR is used to diagnose the electron beam. As shown in Fig.2, the incoherent OTR is split into two beams, one to image the electron bunch transverse spatial distribution, the other to image the angular distribution of the OTR, from which electron energy information can be retrieved. If the electron pulse contains structures shorter than OTR emission wavelength, the OTR can be coherent or partially coherent. Therefore the OTR spectrum is the frequency domain interferogram of coherent OTR light pulses and give temporal information of electron bunch structure [16]. As shown in Fig.2, the OTR emission is also delivered to a spectrometer for electron bunch diagnostic.

To measure the average energy of multi-GeV electrons, a calorimeter, consisting of a periodic structure of He gas chambers and Pb plates, is employed. A high energy electron incident on calorimeter deposits its energy in the Pb plate by generating an electron gamma ray shower (EGS) as well as positrons. These low energy particles enter the He gas chamber, ionize He gas and generate ionization pairs. Applying bias voltage on the He chamber, electronic signals from these ionization pairs can be measured. Simulation results for the ionization pairs produced in the EGS process in a calorimeter are shown in Fig.5. By comparing the variation of the numbers of ionization pairs produced in each He chamber, energy of the electron can be deduced. This calorimeter will be independently calibrated with monoenergetic electron beams of known energy.

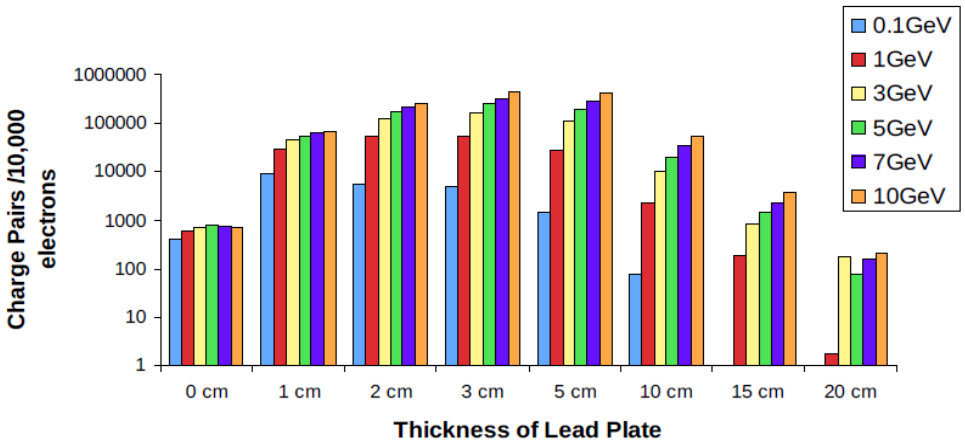

FIGURE 5. EGS simulation of the calorimeter.

CONCLUSIONS

Simulation results show that the TPW laser beam can be self-guided up to 9cm in the plasma "bubble" regime in plasma of density ~10^{17} cm^{-3}, whereupon the bubble oscillates in length, captures ~1nC electrons and accelerates them to 7GeV with less than 10% energy spread. Optical diagnostics, i.e. side TS of main laser beam, transverse interferometry and FDH, are very promising to show experimental evidence for laser self-guiding, and plasma bubble evolution. Electron beam diagnostics, including OTR and calorimetry, can provide very useful information of the electron beam energy, spatial and temporal profiles.

ACKNOWLEDGMENTS

This work was supported by U.S. DoE grants DE-FG03-96ER40954 and DE-FG02-07ER54945. The authors wish to thank Vladimir Khudik and Laura Loiacono for very useful discussions.

REFERENCES

1. J. Rosenzweig, B. Breizman et al., *Phys. Rev*. A **44**, R6189 (1991).
2. A. Pukhov and J. Meyer-ter-Vehn, *Appl. Phys*. B **74,** 355-361 (2002).
3. C. G. R. Geddes et al., *Nature* **431,** 538–541 (2004).
4. J. Faure et al., *Nature* **431,** 541–544 (2004).
5. W. P. Leemans and E. Esarey, *Phys. Today*, 44-49 (March 2010).
6. W. P. Leemans et al., *Nature Phys*. **2**, 696-699 (2006).
7. A. G. R. Thomas et al., *Phys. Rev. Lett.* **100,** 255002 (2008).
8. W. Lu et al., *Phys. Rev. ST Accel. Beams* **10,** 061301 (2007).
9. S. Y. Kalmykov et al., *New J. Phys.* **12**, 045019 (2010).
10. E. Gaul et al., *Appl. Opt*. **49**, 1676-1681 (2010).
11. S. Y. Kalmykov et al., *Phys. Rev. Lett.* **103**, 135004 (2009).
12. N. H. Matlis et al., *Nature Phys.* **2**, 749-753 (2006).
13. P. Monot et al., *Phys. Rev. Lett.* **74**, 2953-2956 (1995).
14. R. Wagner et al., *Phys. Rev. Lett*.**78**, 3215-3218 (1997)
15. N. E. Andreev et al., *New J. Phys.***12**, 045024 (2010).
16. Y. Glinec et al., *Phys. Rev. Lett.* **98**, 194801 (2007).